The impact of Miocene atmospheric carbon dioxide fluctuations on climate and the evolution of terrestrial ecosystems

Wolfram M. Kürschner*†, Zlatko Kvaček‡, and David L. Dilcher§

*Faculty of Science, Institute of Environmental Biology, Department of Palaeoecology, Laboratory of Palaeobotany and Palynology, Utrecht University, Budapestlaan 4, 3584 CD, Utrecht, The Netherlands; ‡Faculty of Natural Sciences, Charles University, Albertov 6, 128 43 Prague 2, Czech Republic; and §Florida Museum of Natural History, University of Florida, Gainesville, FL 32611-7800

Edited by Robert A. Berner, Yale University, New Haven, CT, and approved November 6, 2007 (received for review September 10, 2007)

The Miocene is characterized by a series of key climatic events that led to the founding of the late Cenozoic icehouse mode and the dawn of modern biota. The processes that caused these developments, and particularly the role of atmospheric CO_2 as a forcing factor, are poorly understood. Here we present a CO_2 record based on stomatal frequency data from multiple tree species. Our data show striking CO_2 fluctuations of ≈600–300 parts per million by volume (ppmv). Periods of low CO_2 are contemporaneous with major glaciations, whereas elevated CO_2 of 500 ppmv coincides with the climatic optimum in the Miocene. Our data point to a long-term coupling between atmospheric CO_2 and climate. Major changes in Miocene terrestrial ecosystems, such as the expansion of grasslands and radiations among terrestrial herbivores such as horses, can be linked to these marked fluctuations in CO_2.

atmospheric CO_2 | fossil plants | paleoclimates | stomata | C_4 plants

The Miocene is distinguished by extreme climatic optima alternating with major long-term climatic cooling, which together mark the founding of the modern late Cenozoic cold mode and the evolution of modern terrestrial biomes (1). Grass-dominated ecosystems became established in the low and middle latitudes of many parts of the world, such as North America, Eurasia, Africa, and Australia (2). Major radiations in large mammalian herbivores have been attributed to changes in the distribution of vegetation and terrestrial primary productivity (3–5). A significant change in dental morphology from low- to high-crowned toothed horses occurs during the middle Miocene, whereas a transition from a C_3 plant to C_4 plant diet did not take place before the late Miocene (6).

Both Cenozoic climate trends and changes in terrestrial ecosystems have been thought to be influenced by long-term CO_2 fluctuations (6–8). Before marine pCO_2 proxy records were available, Cenozoic CO_2 trends were inferred from carbon-isotope records of paleosols (9) and from carbon cycling models (10), which indicated a long-term decrease from ≈1,000 to <500 parts per million by volume (ppmv) throughout the Cenozoic. Approximately a decade later, CO_2 reconstructions based on marine geochemical proxies indicated consistently low late Pleistocene (glacial-like) CO_2 values of ≈200–280 ppmv (11, 12). Consequently, the Miocene has been regarded as a geological period in which climate and the carbon cycle were essentially decoupled. Because of this alleged decoupling, the role of atmospheric CO_2 as a climate forcing factor has been disputed (13–15). However, a permanently low CO_2 scenario has been challenged because photosynthetic models predict that plant life would not have thrived under such conditions (16). Climate models showed the importance of atmospheric CO_2 as a fundamental boundary condition for Cenozoic climate change (17). In fact, a coupling between atmospheric CO_2 and glacial–interglacial cycles over the past 600,000 years is well documented by ice core analysis (18). Understanding the long-term perspective beyond the Pleistocene is essential because climate and CO_2 fluctuations on progressively shorter time scales are ultimately dependent on the evolution of the global carbon cycle and earth's climate on longer time scales. Recently, refined geochemical studies of marine and terrestrial sedimentary records suggest a coupling between atmospheric CO_2 and temperature over Phanerozoic time scales (19–21).

In addition to geochemical CO_2 proxies, stomatal frequency analysis on fossil leaf remains represents a terrestrial proxy for CO_2 that is based on the inverse relationship between atmospheric CO_2 and stomatal frequency (22). In the present study, stomatal frequency is expressed as the stomatal index (*SI*), which is calculated as $SI\ (\%) = [SD/(SD + ED)] \times 100$, where SD is the stomatal density and ED is the epidermal cell density. Because *SI* normalizes for leaf expansion, it is largely independent of plant water stress and is primarily a function of CO_2 (22, 23). Calculation of *SI* provides a robust method for estimating CO_2 levels on short (24) and geologically long time scales (25, 26). Because the stomatal frequency response to CO_2 is species-specific, quantitative estimates of CO_2 are limited to extant species. Here we present a CO_2 reconstruction based on a multiple-species stomatal frequency record from leaf remains of two extant lineages of laurel species (the *Laurus abchasica* and *Laurus nobilis* lineage and the *Ocotea hradekensis* and *Ocotea foetens* lineage), maidenhair tree (*Ginkgo biloba*), and an extinct laurel species (*Laurophyllum pseudoprinceps*). For each extant species, the stomatal frequency response has been independently calibrated based on historical sets of herbarium leaf material, using standard protocols (27). The training datasets and CO_2 inference models, respectively, for *L. nobilis* and *O. foetens* are shown in Figs. 1 and 2 (for details, see *Material and Methods*). The *SI* calibration for the extinct species *L. pseudoprinceps* has been established by cross-calibration with known CO_2 levels from those stratigraphic units in which it occurs together with the extant laurel species and *Ginkgo*.

We address two main questions in this article: (*i*) What was the relationship between the long-term CO_2 fluctuations and climate evolution during the Miocene? and (*ii*) Was CO_2 an environmental stress factor that influenced the evolution of modern terrestrial ecosystems?

Results and Discussion

Fossil *SI*s of all four species (*L. pseudoprinceps*, *L. nobilis*, *O. foetens*, and *G. biloba*) show pronounced fluctuations over the

Author contributions: W.M.K. designed research; W.M.K., Z.K., and D.L.D. performed research; W.M.K. analyzed data; and W.M.K. and D.L.D. wrote the paper.

The authors declare no conflict of interest.

This article is a PNAS Direct Submission.

See Commentary on page 407.

†To whom correspondence should be addressed. E-mail: w.m.kuerschner@uu.nl.

This article contains supporting information online at www.pnas.org/cgi/content/full/0708588105/DC1.

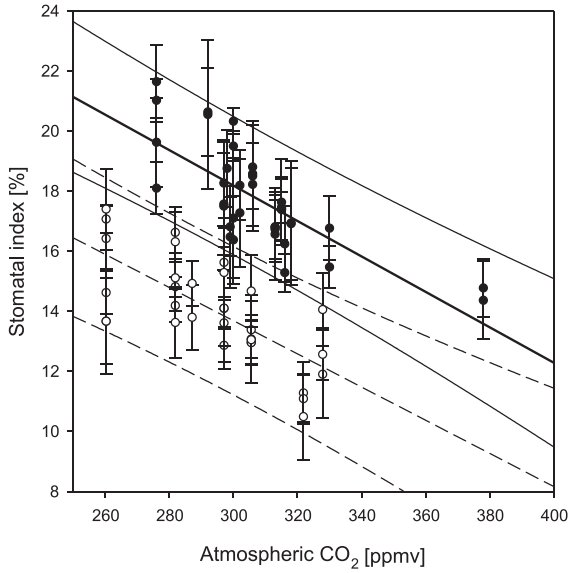

Fig. 1. Training dataset of mean *SI* values of *L. nobilis* (filled circles) and *O. foetens* (open circles) vs. atmospheric CO_2 levels with 95% prediction interval. Error bars show standard deviation.

time interval studied (Fig. 3*A*). Three periods can be recognized in the present record. During the oldest period—the late Oligocene to early Miocene (25–20 Ma)—the *SI* of *L. pseudoprinceps* shows a significant increase from ≈9% to 15% and remains high during the early Miocene. During the middle period—the late early to early middle Miocene (20–16 Ma)—*L. pseudoprinceps* shows a decrease in *SI* from 15% to 12%. A simultaneous decline in *SI* is found for two other laurel species, *L. nobilis* and *O. foetens*, from 12% to 10% and from 12% to 8%, respectively. In the youngest period of the present study—the middle Miocene (16–12 Ma)—*L. nobilis* shows a marked increase from 10% to 20%, followed by a decrease to 14% during the late middle Miocene. The pronounced increase in the *SI* of *L. nobilis* during the early middle Miocene is confirmed by a sharp shift in the *SI* of *G. biloba* from 8% to 15%.

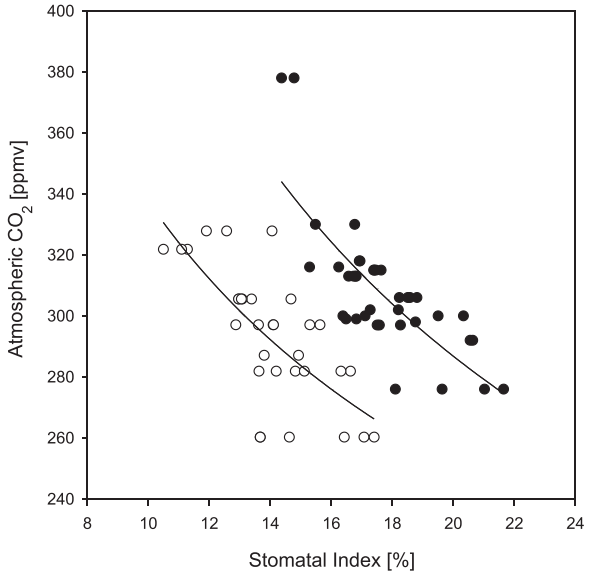

Fig. 2. CO_2 inference model based on historical series of herbarium sheets for *L. nobilis* (filled circles) and *O. foetens* (open circles).

The *SI* record of the present study reveals prominent changes in CO_2 since the late Oligocene (Fig. 3*B*). CO_2 declines drastically, from ≈600 to ≈340 ppmv, during the Oligocene–Miocene transition. It remains low (at about this level) until the middle early Miocene. From ≈20 Ma, CO_2 increases again to reach a maximum of ≈400–500 ppmv in the early middle Miocene (15.5 Ma). Superimposed on this rising trend are several smaller, temporary CO_2 oscillations with amplitude of ≈50 ppmv. A second major CO_2 decrease to 280 ppmv occurs during the middle Miocene (15.5–14 Ma), followed by a slight increase to ≈340 ppmv during the late Miocene. A previous CO_2 reconstruction based on North American leaf remains (26) fit perfectly into the present study, but it represented only a few measurements at ≈15 Ma.

It should be noted that because of the nonlinear nature of stomatal frequency response, the sensitivity of this proxy decreases at high CO_2 levels (greater than or equal to ≈400 ppmv). Consequently, the high CO_2 levels during the climate optima at ≈22 Ma and 15.5 Ma may represent a conservative estimation rather than the average CO_2 level. Despite the applied log-transformation, the CO_2 inference models (Eqs. **3** and **4** in *Materials and Methods*) underestimate the actual CO_2 levels at extrapolation far beyond the calibration interval. To estimate this uncertainty, the CO_2 levels predicted by the inference models are plotted vs. the input CO_2 values used to establish the transfer functions (Fig. 4). At ≈500 ppmv CO_2, the inference models of *L. nobilis* and *O. foetens* underestimate the CO_2 value by ≈150 and 200 ppmv, respectively. Consequently, the atmospheric CO_2 levels during the middle Miocene climatic optimum would have been closer to ≈650–700 ppmv than to the uncorrected value of ≈500 ppmv. During the late Oligocene, climate optimum CO_2 levels would have been 800–900 ppmv, rather than the uncorrected 600 ppmv, which is intriguingly close to the estimates provided by the alkenone-based CO_2 proxy record (14). Moreover, well preserved leaf material is rare, and the number of observations per individual sample is (at the present stage) in some cases rather low. However, the largest portion, 70%, of the CO_2 record is based on stomata counts from the three extant species that are independently calibrated. Different species show the same trends, which reinforces the fidelity of the reconstructed CO_2 trends through the Miocene. All in all, our data do not show any signs of a prolonged Miocene low-CO_2 scenario, as suggested by geochemical proxy records (11, 12, 14). If such a scenario had existed, it should also be evident in the present study because the botanical proxy used is sensitive to low CO_2 levels (22).

The present leaf-based CO_2 reconstruction shows a similar CO_2 decline at the Oligocene–Miocene transition as in the marine proxy records (12, 14), but it deviates significantly throughout the course of the Miocene. The alkenone-based CO_2 record indicates consistently low Pleistocene-like CO_2 levels (200–280 ppmv) and shows hardly any covariation with Miocene climate fluctuations. The boron isotope-based CO_2 reconstruction shows a decrease in atmospheric CO_2 ≈15 Ma, which is in the order of the present study (≈150 ppmv), although the absolute values are significantly lower (by ≈200 ppmv) than in our study. However, our results provide evidence from the terrestrial fossil record that CO_2 had a profound influence on the Miocene long-term climate evolution as recorded in marine records (1) (Fig. 3*C*). Despite the limited temporal resolution of the present study, CO_2 fluctuations correlate with some of the climate events (Mi1/1b, Mi2, and Mi3/4) known from the marine oxygen isotope curve (1). In the future, leaf-based CO_2 reconstructions with a finer time resolution may could potentially reveal patterns of higher order fluctuations that are coupled to orbital cycles, as suggested by marine proxy records (28). The global mean temperature model shows a 2–3°C decline during the early Miocene and middle Miocene climate events (Fig. 3*C*).

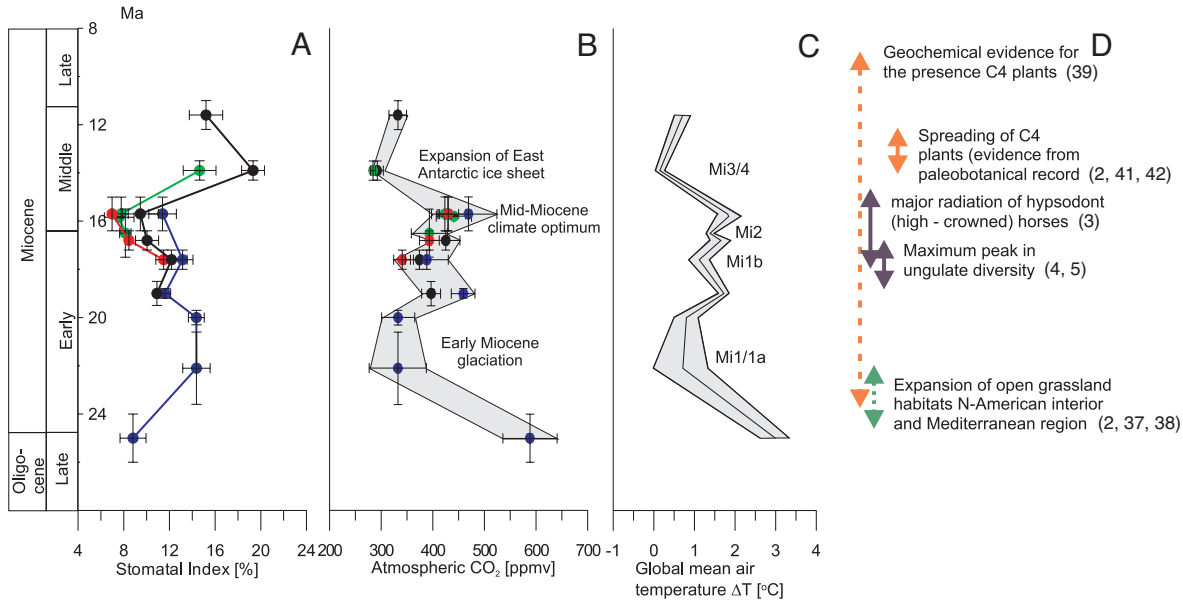

Fig. 3. Late Oligocene–Miocene stomatal index records, inferred atmospheric CO_2 fluctuations, and effects on global temperature compared with major events in terrestrial ecosystems. (*A*) *SI* of fossil leaf remains between 25 and 12 Ma (late Oligocene until late middle Miocene. For a list of locations and their age assessment, see SI Table 3). The lines represent trends in *SI*: blue, *L. pseudoprinceps*; black, *L. nobilis*; red, *O. foetens*; green, *G. biloba*. The values represent means per stratigraphic unit, with error bars indicating the standard deviation of the *SI*. The age error bars indicate the minimum and maximum ages of the sample. The stratigraphic framework is established by vertebrate biostratigraphy and magnetostratigraphy (see also SI Table 3). (*B*) Reconstructed late Oligocene–middle Miocene CO_2 levels based on individual independently calibrated tree species. The error bars of the species-specific CO_2 estimates are based on the standard deviation of the *SI* measurements on individual fossil leaf samples. The gray band indicates the envelope as determined by the minimum and maximum CO_2 levels inferred from all individual samples per stratigraphic unit. (*C*) Modeled temperature departure of global mean surface temperature from present day, calculated from mean CO_2 estimates by using a CO_2–temperature sensitivity study (46). Also indicated are the major Miocene climate key events and the position of the Miocene cooling events Mi1/1a, Mi1b, Mi2, and Mi3/4 known from the marine oxygen isotope record (1). The effects of pCO_2 level changes on the global mean land surface temperature were estimated assuming a radiative relationship between CO_2 mixing and global air temperature inferred from climate–CO_2 sensitivity models expressed as $\Delta T = 4\ln(C/CO)$, where C is the mixing ratio and CO is the preindustrial CO_2 mixing ratio of 278 ppmv (46). (*D*) Major events in the terrestrial ecosystems in response to the Miocene CO_2 trends, such as changes in terrestrial herbivore communities (3–5), the expansion of Miocene grasslands (2, 37, 38), and evidence for C_4 biomass from paleosols (43).

Our data confirm modeling experiments that show that Cenozoic CO_2 must decline below a threshold of ≈500 ppmv to induce significant buildup of Antarctic ice sheets (17). Unlike the geochemical proxy records (11, 12, 14), our data indicate that elevated CO_2 levels contributed to the middle Miocene climatic optimum. Several lines of evidence from the fossil and geological record (15, 29–32) suggest that this time interval (≈14.5–17 Ma) was the warmest period of the past 35 Ma. Our results demonstrate that this climate optimum was forced significantly by elevated CO_2 levels similar to those, for example, during the early Eocene (12, 14, 26). A likely source of the late, early, and middle Miocene CO_2 increases was extensive volcanic activity during the Columbia River Flood Basalt volcanism and the Central European volcanism (33). The marked CO_2 drop during the Miocene, in turn, may be the result of increased C_{org} burial resulting from the Himalayan uplift (34) and/or of enhanced marine productivity in the Pacific ocean (7) and the global occurrence of vast brown-coal-forming basins (35).

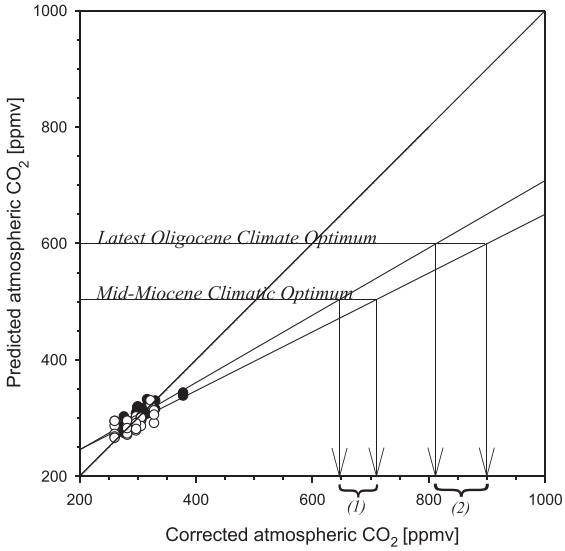

Fig. 4. Predicted CO_2 concentrations calculated from Eqs. **3** and **4** for *L. nobilis* (filled circles) and *O. foetens* (open circles), plotted vs. the actual atmospheric CO_2 levels with a linear extrapolation to elevated CO_2. The arrows indicate the value of the corrected CO_2 level for the climatic optima in the middle Miocene (*1*) and latest Oligocene (*2*).

The marked Miocene CO_2 variations may have directly impacted the structure and productivity of terrestrial biomes by affecting plant photosynthetic performance. In sensitivity tests at 280 and 560 ppmv for Miocene global vegetation models (36), CO_2 shows pronounced changes related to vegetation distribution with regard to the degree of tree coverage for the seasonal dry tropics. However, evidence from the fossil record for the global distribution pattern of these biomes in the Miocene is rather scattered because fossil plant assemblages are highly influenced by taphonomical processes. Phytolith studies from the North American continental interior have shed new light on Miocene vegetational history (37). They reveal that pronounced changes in vegetation took place at the Oligocene–Miocene transition. Late Oligocene vegetation was a closed forest with palm and bamboo understory, whereas early Miocene plant communities were characterized by a mix of C_3 grasses and

herbs, forming savannas or open woodland habitats (37). Recently, phytolith studies from the eastern Mediterranean region reveal that relatively open, grass-dominated habitats were established by at least the early Miocene (38). Intriguingly, these examples from the fossil record are similar to changes in vegetation distributions that occur in the Miocene global vegetation models as the result of CO_2 sensitivity runs (36). Growth experiments and vegetation models with modern mixed tree/grass ecosystems show that changes in atmospheric CO_2 directly affect tree cover by modifying water relationships in herbaceous vs. woody plants (39) or by modifying the (re)growth rates of plants recovering after a disturbance such as wildfire (40). Therefore, the opening of the forest vegetation and proliferation of open grassland habitat may have been influenced by the initial CO_2 drawdown to ≈300 ppmv during the early Miocene (Fig. 3*D*). After a continuous CO_2 increase up to ≈550 ppmv between 20 and 16 Ma, a second major drop in CO_2 at ≈12 Ma down to ≈280 ppmv may have increased the environmental stress induced by CO_2 starvation. We hypothesize that under these CO_2-limiting conditions, in concert with an open habitat, exposure of grasses to high light intensity and water-stressed environments, combined with the coevolution of herbivores, may have facilitated the first radiation of C_4 grasses. To date, the fossil record of C_4 plants is still rather enigmatic. A few paleobotanical studies reveal evidence for C_4 plants in the middle Miocene (41, 42), whereas geochemical data suggest their presence since the early Miocene (43). Another line of evidence on the origin of C_4 plants comes from the molecular clock approach, which estimates an approximate maximum age for the origin of modern C_4 plants of 25 Ma (44). These data coincide approximately with the CO_2 drop in the early Miocene. Carbon isotope records of paleosols and fossil tooth enamel indicate, however, that the major proliferation of C_4 grasslands did take place during the late Miocene, ≈8 Ma ago (6). The later vegetation change has been attributed to an increased seasonality and increased fire frequency (45).

Changes in the productivity and species richness of terrestrial vegetation must have affected herbivore communities. Hoofed herbivorous large mammals on the North American continent show a maximum diversity during the middle Miocene climatic optimum (4, 5) (Fig. 3*D*). This maximum in both local and regional diversity greatly exceeds the diversity of ungulates in any present-day habitat, which implies a greater primary productivity than is seen today. Preliminary review data suggest that the pattern of elevated ungulate diversity is a global phenomenon, and, therefore, a global driving force is the most likely explanation. CO_2 fertilization during the middle Miocene climatic optimum may have made possible the expansion of high-productivity terrestrial biomes that supported high-diversity browser communities.

As a result of climatic changes such as increased seasonality and cooling, as well as the decline in primary productivity due to the marked post-middle Miocene CO_2 crisis, woodland biomes retreated, the species richness of browsing mammals declined, and grazers increased their diversity (3). A large number of terrestrial mammalian herbivores, such as equids, camelids, antilocaprids, rhinos, and proboscideans show dramatic morphological changes of their dentitions during the Miocene (3–5). In particular, early Cenozoic horses are characterized by brachydont (short-crowned) dentitions but show, from the late middle Miocene on (≈15 Ma), a rapid diversification of hypsodont (high-crowned) taxa, which has been attributed as an adaptation to include more fibrous and abrasive material, such as grasses, in the diet (3). This development implies the coevolution of large herbivores and plants in response to Miocene climate and atmospheric CO_2 fluctuations.

Materials and Methods

Standardized computer-aided determinations of epidermal parameters were performed on an AnalySIS image analysis system (Soft Imaging Systems) software. All statistics and graphs were made with Sigmaplot version 9.1 (Systat Software). On average, 5–10 stomata-bearing alveoles per leaf sample were measured for ED (n/mm^2) and SD (n/mm^2). From SD and ED, the area-independent *SI* was calculated: $SI\ (\%) = [SD/(SD + ED)] \times 100$. Most of the cuticle preparations (stored at Charles University) were collected from several brown-coal basins in the Czech Republic (Most and Zitava basins, South Bohemia), supplemented with some material from Austria (Parschlug Basin, Styria) and Germany (Lower Rhine Embayment, Lausitz Basin). References for the age assessments of the individual fossil leaf samples are given in supporting information (SI) Table 3.

A total of 68 herbarium leaf samples (see SI Tables 1 and 2) and 36 fossil leaf samples (SI Table 3) were studied for their epidermal cell properties. The data shown in SI Tables 1–3 represent means with standard deviation per herbarium leaf or fossil leaf remains, respectively. The species included are the extant taxa *L. abchasica*, *O. hradekensis*, and *G. biloba*, as well as one extinct species, *L. pseudoprinceps*. To convert the *SI* values from the extant species *L. abchasica* and *O. hradekensis* to atmospheric CO_2 levels, CO_2 inference models were established from their living equivalents, *L. nobilis* and *O. foetens* (Figs. 1 and 2), from historical herbarium sheets collected over the 19th and 20th centuries, covering the CO_2 increase since the industrial revolution. Historical atmospheric CO_2 concentrations used for calibration are annual means as measured on Mauna Loa, HI, since 1952 (47), supplemented by CO_2 measurements from Antarctic ice cores (Siple Station) (48). The taxonomical relationships have been established by extensive comparative studies on leaf morphology and cuticle anatomy (49–51). CO_2 estimates from *G. biloba* were based on calibration data by Royer *et al.* (26). In the absence of a modern equivalent for the extinct species *L. pseudoprinceps*, the *SI* response of this species has been cross-calibrated by using Miocene CO_2 levels inferred from the three extant species.

The *SI* calibration of *L. nobilis* to atmospheric CO_2 concentrations results in a linear relationship, with

$$SI = -0.059\ CO_2 + 35.876 \qquad [1]$$

and a coefficient of determination (R^2) of 0.56.

The *SI* calibration of *O. foetens* to atmospheric CO_2 concentrations results in a linear relationship, with

$$SI = -0.0552\ CO_2 + 30.245 \qquad [2]$$

and an R^2 of 0.5.

To account for the nonlinear response of *SI* to changing CO_2 concentrations, both herbarium *SI* data and the historical CO_2 concentrations are log-transformed before fitting a linear response curve through the datasets. For *L. nobilis*, this results in a relationship of

$$CO_2 = 10^{3.173} - [0.5499 \times \log(SI_{fossil})], \qquad [3]$$

with an R^2 of 0.78 between measured and inferred CO_2 values and a root mean square error (RMSE) of 13.5 ppmv CO_2.

For *O. foetens*, the regression curve (Fig. 2) and statistics are

$$CO_2 = 10^{2.9567} - [0.4284 \times \log(SI_{fossil})], \qquad [4]$$

with an R^2 of 0.5 between measured and inferred CO_2 values and an RMSE of 16 ppmv CO_2.

In the absence of a modern equivalent for the extinct species *L. pseudoprinceps*, the *SI* response of this species has been cross-calibrated by using Miocene CO_2 levels inferred from the three extant species. This results in a relationship of

$$CO_2 = -46.011 \times SI_{fossil} + 993.37, \qquad [5]$$

with an R^2 of 0.68.

The multiple-species *SI* record based on three extant species allows that CO_2 values are independently inferred from the individual species-specific CO_2 inference models and verified for interspecific coherence.

O. foetens is an endemic tree from Madeira and the Canary Islands. It occurs over a wide range of altitudes in valleys and hills of the interior of the islands and is the highest tree of the laurel forest (Larissilva). Because the historical herbarium leaves were collected at different altitudes from approximately sea level up to 1,000 m, the stomatal frequency response is expressed against the

CO_2 partial pressure and corrected for the altitude at which leaves were collected (see SI Table 2).

The atmospheric CO_2 partial pressure was calculated with Eqs. **6** and **7** (52, 53). Atmospheric pressure decreases with altitude in a predictable manner,

$$P_{\mathrm{air},\,z} = 101{,}325^{[\mathrm{MW(air)}\cdot g\cdot z/RT]}, \qquad [6]$$

where $MW_{(air)}$ is the molecular weight of air (28.964×10^{-3} kg/mol), z is altitude in meters, g is acceleration due to gravity in meters per second, R is the gas constant (8.3144 J/mol), and T is mean July temperature in kelvin.

The CO_2 partial pressure depends on the altitude, with

$$P_{\mathrm{CO}_{2,\,z}} = [P_{\mathrm{air},\,z}/101{,}325]\cdot P_{\mathrm{CO}_{2,\,\mathrm{sea\ level}}}, \qquad [7]$$

where $P_{CO_{2,\,z}}$ is the CO_2 partial pressure at altitude z, and $P_{CO_{2,\,sea\ level}}$ is the CO_2 partial pressure at sea level.

To calculate CO_2 estimates in mixing ratios (ppmv), the altitude-corrected CO_2 partial pressure values of the *O. foetens* training set were reconverted into mixing ratios at sea level with

$$C_{\mathrm{CO}_2} = (P_{\mathrm{CO}_{2,\,\mathrm{sea\ level}}}/101{,}325)\cdot 10^6, \qquad [8]$$

where C_{CO_2} is the mixing ratio in ppmv, and $P_{CO_{2,\,sea\ level}}$ is the partial pressure at sea level.

ACKNOWLEDGMENTS. We thank F. Wagner, H. Visscher, T. Lott, and two anonymous reviewers for thoughtful comments and the National Herbarium of The Netherlands, Leiden, for providing laurel herbarium sheets. This work was supported by the European Science Foundation (Research Networking Program: Environments and Ecosystem Dynamics of the Eurasian Neogene), the Grant Agency of the Czech Republic Grant CR 205/04/0099 (to W.M.K. and Z.K.), the Florida Museum of Natural History and the Becker/Dilcher Research Fund (D.L.D.), and the Alexander von Humboldt Stiftung (W.M.K.). This is publication no. 20071101 of the Netherlands Research School of Sedimentary Geology and no. 605 of Contributions in Paleontology, Florida Museum of Natural History.

1. Zachos JC, Pagani M, Sloan L, Thomas E, Billups K (2001) *Science* 292:686–693.
2. Jacobs JC, Kingston JD, Jacobs LL (1999) *Ann Missouri Bot Gard* 86:590–643.
3. MacFadden BJ (2005) in *A History of Atmospheric CO_2 and its Effects on Plants, Animals, and Ecosytems*, eds Ehleringer JR, Cerling TE, Dearing MD (Springer, Berlin), Ecological Studies Series, Vol 177, pp 273–292.
4. Janis CM, Damuth J, Theodor JM (2000) *Proc Natl Acad Sci USA* 97:7899–7904.
5. Janis CM, Damuth J, Theodor JM (2004) *Palaeogeogr Palaeoclimatol Palaeoecol* 207:371–398.
6. Cerling TE, Harris JM, MacFadden BJ, Leacey MG, Quade J, Eisenmann V, Ehleringer JR (1997) *Nature* 389:153–158.
7. Vincent E, Berger WH (1985) in *The Carbon Cycle and Atmospheric CO_2: Natural Variations Archean to Present*, eds Sundquist ET, Broecker WS (Am Geophys Union, Washington), Vol 32, pp 455–468.
8. Raymo ME (1991) *Geology* 19:344–347.
9. Cerling TE (1991) *Am J Sci* 291:377–400.
10. Berner RA (1991) *Am J Sci* 291:339–376.
11. Pagani M, Arthur MA, Freeman KH (1999) *Paleoceanography* 14:273–292.
12. Pearson PN, Palmer MR (2000) *Nature* 406:695–699.
13. Shevenell AE, Kennett JP, Lea DW (2004) *Science* 305:1766–1770.
14. Pagani M, Zachos JC, Freeman KH, Tipple B, Bohaty S (2005) *Science* 309:600–603.
15. Mosbrugger V, Utescher T, Dilcher DL (2005) *Proc Natl Acad Sci USA* 102:14964–14969.
16. Cowling SA (1999) *Science* 285:1500–1501.
17. DeConto RM, Pollard D (2003) *Nature* 421:245–249.
18. Siegenthaler U, Stocker TF, Monnin E, Luethi D, Schwander J, Stauffer B, Raynaud D, Barnola J-M, Fischer H, Masson-Delmotte V, Jouzel J (2005) *Science* 310:1313–1317.
19. Montanez IP, Tabor NJ, Niemeier D, DiMichele WA, Frank TD, Fielding CR, Isbell JL, Birgenheier LP, Rygel MC (2007) *Science* 315:87–91.
20. Came RE, Eiler JM, Veizer J, Azmy K, Brand U, Weidman CR (2007) *Nature* 449:198–202.
21. Royer DL, Berner RA, Park J (2007) *Nature* 446:530–532.
22. Woodward FI (1987) *Nature* 327:617–618.
23. Kürschner WM (1997) *Rev Palaeobot Palynol* 96:1–30.
24. Wagner F, Bohncke SJP, Dilcher DL, Kürschner WM, van Geel B, Visscher H (1999) *Science* 284:1971–1973.
25. van der Burgh J, Visscher H, Dilcher DL, Kürschner WM (1993) *Science* 260:1788–1790.
26. Royer DL, Wing SL, Beerling DJ, Jolley DW, Koch PL, Hickey LJ, Berner RA (2001) *Science* 292:2310–2313.
27. Wagner F, Dilcher DL, Visscher H (2006) *Am J Bot* 92:690–695.
28. Holbourn A, Kuhnt W, Schulz M, Erlenkeuser H (2005) *Nature* 438:483–487.
29. White JM, Ager TA, Adam DP, Leopold EB, Liu G, Jetté H, Schweger CE (1997) *Palaeogeogr Palaeoclimatol Palaeoecol* 130:293–306.
30. Boehme M (2003) *Palaeogeogr Palaeoclimatol Palaeoecol* 195:389–401.
31. Zou H, McKeegan KD, Xu X, Zindler A (2004) *Chem Geol* 207:101–116.
32. Flower BP, Kennett JP (1994) *Palaeogeogr Palaeoclimatol Palaeoecol* 108:537–555.
33. Hodell DA, Woodruff F (1994) *Paleoceanography* 9:405–426.
34. France-Lanord C, Derry LA (1997) *Nature* 390:65–67.
35. Holdgate GR, Clarke JDA (2000) *AAPG Bull* 84:1129–1151.
36. Francois L, Ghislain M, Otto D, Micheels A (2006) *Palaeogeogr Palaeoclimatol Palaeoecol* 238:302–320.
37. Stroemberg CAE (2004) *Palaeogeogr Palaeoclimatol Palaeoecol* 207:239–275.
38. Stroemberg CAE, Werdelin L, Friis EM, Saraç G (2007) *Palaeogeogr Palaeoclimatol Palaeoecol* 250:18–49.
39. Polley HW, Johnson HB, Tischler CR (2002) *Plant Ecol* 164:85–94.
40. Bond WJ, Midgley GF, Woodward FI (2003) *Global Change Biol* 9:973–982.
41. Tidwell WD, Nambudiri EMV (1989) *Rev Palaeobot Palynol* 60:165–177.
42. Kingston JD, Marino BD, Hill A (1994) *Science* 264:955–959.
43. Fox DL, Koch PL (2003) *Geology* 31:809–812.
44. Sage RF (2004) *New Phytol* 161:341–370.
45. Beerling DJ, Osborn CP (2006) *Global Change Biol* 12:2023–2031.
46. Kothavala Z, Oglesby RJ, Saltzman B (1999) *Geophys Res Lett* 26:209–212.
47. Keeling CD, Whorf TP (2003). *Atmospheric CO_2 Concentrations—Mauna Loa Observatory, Hawaii, 1958–2003*. Available at http://cdiac.ornl.gov/pns/pns_main.html.
48. Neftel AH, Friedli E, Moor H, Lötscher H, Oeschger H, Siegenthaler U, Stauffer B (1994) in *Trends: A Compendium of Data on Global Change* (Carbon Dioxide Information Analysis Center, Oak Ridge National Lab, US Dept of Energy, Oak Ridge, TN). Available at http://cdiac.ornl.gov/trends/co2/contents.htm.
49. Ferguson DK (1974) *Bot J Linnean Soc* 68:51–72.
50. Kvaček Z (1971) *Sbor Geol Věd, Paleont* 13:47–86.
51. Kvaček Z, Bůžek Č (1966) *Věst Ústř Úst Geol* 41:291–294.
52. Jones HG (1992) *Plants and Microclimate* (Cambridge Univ Press, Cambridge, UK).
53. McElwain JC (2004) *Geology* 32:1017–1020.